HHS Public Access

Author manuscript

Science. Author manuscript; available in PMC 2023 October 31.

Published in final edited form as:

Science. 2023 June 30; 380(6652): 1372–1380. doi:10.1126/science.abn1725.

Metabolic orchestration of cell death by AMPK-mediated phosphorylation of RIPK1

Tao Zhang[1,†], **Daichao Xu**[2,3,†,*], **Elijah Trefts**[4,†], **Mingming Lv**[1,†], **Hiroyuki Inuzuka**[1], **Guobin Song**[5], **Min Liu**[6], **Jianlin Lu**[7], **Jianping Liu**[2], **Chen Chu**[8,9], **Min Wang**[10], **Huibing Wang**[3], **Huyan Meng**[11], **Hui Liu**[1], **Yuan Zhuang**[12], **Xingxing Xie**[2], **Fabin Dang**[1], **Dongxian Guan**[5], **Yuqin Men**[5], **Shuwen Jiang**[13,5], **Cong Jiang**[1], **Xiaoming Dai**[1], **Jing Liu**[1], **Zhen Wang**[1], **Peiqiang Yan**[1], **Jingchao Wang**[1], **Zhenbo Tu**[1], **Mrigya Babuta**[12], **Emily Erickson**[1], **Alissandra L. Hillis**[1], **Christian C. Dibble**[1], **John M. Asara**[14], **Gyongy Szabo**[12], **Piotr Sicinski**[8,9,15], **Ji Miao**[5], **Yu-Ru Lee**[16], **Lifeng Pan**[17,*], **Reuben J. Shaw**[4,*], **Junying Yuan**[2,3,*], **Wenyi Wei**[1,*]

[1]Department of Pathology, Beth Israel Deaconess Medical Center, Harvard Medical School, Boston, MA 02215, USA

[2]Interdisciplinary Research Center on Biology and Chemistry, Shanghai Institute of Organic Chemistry, Chinese Academy of Sciences, 201203 Shanghai, China

[3]Department of Cell Biology, Harvard Medical School, Boston, MA 02115, USA

[4]The Salk Institute for Biological Studies, La Jolla, CA 92037, USA

[5]Division of Endocrinology, Boston Children's Hospital, Harvard Medical School, Boston, MA 02115, USA

[6]Transfusion Medicine, Boston Children's Hospital, Harvard Medical School, Boston, MA 02115, USA

[7]Department of Immunology, St. Jude Children's Research Hospital, Memphis, TN 38105, USA

[8]Department of Cancer Biology, Dana-Farber Cancer Institute, Boston, MA 02215, USA

[9]Department of Genetics, Blavatnik Institute, Harvard Medical School, Boston, MA 02115, USA

[*]Corresponding author. xudaichao@sioc.ac.cn (D.X.); panlf@sioc.ac.cn (L.P.); shaw@salk.edu (R.J.S.); junying_yuan@sioc.ac.cn (J.Y.); wwei2@bidmc.harvard.edu (W.W.).

[†]These authors contributed equally to this work.

Author contributions: T.Z. was the key contributor in designing and conducting most of the experiments. T.Z., D.X., L.P., R.J.S., J.Y., and W.W. conceived of and directed the project. T.Z., D.X., J.Y., and W.W. wrote the manuscript. D.X., E.T., and M.Lv. conducted key experiments. H.I., G.So., M.Li., J.Lu, Jia.Liu, C.C., M.W., H.W., H.M., H.L., Y.Z., X.X, F.D., D.G., Y.M., S.J., C.J., X.D., Jin.Liu, Z.W., P.Y., J.W., Z.T., M.B., E.E., A.L.H., and J.M.A. conducted some of the experiments. C.C.D., G.Sz., P.S., J.M., and Y.-R.L. commented on and edited the manuscript.

Competing interests: W.W. is a cofounder and consultant for ReKindle Therapeutics. P.S. has been a consultant at Novartis, Genovis, Guidepoint, The Planning Shop, ORIC Pharmaceuticals, Cedilla Therapeutics, Syros Pharmaceuticals, Exo Therapeutics, Curie Bio Operations, Exscientia, Ligature Therapeutics, and Redesign Science; and his laboratory receives research funding from Novartis. G.Sz. is a paid consultant for Cyta Therapeutics, Durect Co, Evive, Merck, Pfizer, Surrozen, Terra Firma, Pandion Therapeutics, LabCorp, Glympse Bio, Satellite Bio, and Zomagen. G.Sz. has additional financial interests in Glympse Bio, Satellite Bio, and Zomagen. The other authors declare that they have no competing financial interests.

View/request a protocol for this paper from Bio-protocol.

[10]Department of Biliary-Pancreatic Surgery, Affiliated Tongji Hospital, Tongji Medical College, Huazhong University of Science and Technology, 430030 Wuhan, Hubei, China

[11]F.M. Kirby Neurobiology Center, Boston Children's Hospital, Boston, MA 02115, USA

[12]Department of Medicine, Beth Israel Deaconess Medical Center, Harvard Medical School, Boston, MA 02215, USA

[13]Department of Metabolic and Bariatric Surgery, The First Affiliated Hospital of Jinan University, 510632 Guangzhou, China

[14]Division of Signal Transduction, Department of Medicine, Beth Israel Deaconess Medical Center, Harvard Medical School, Boston, MA 02215, USA

[15]Department of Histology and Embryology, Center for Biostructure Research, Medical University of Warsaw, 02-004 Warsaw, Poland

[16]Institute of Biomedical Sciences, Academia Sinica, Taipei 115201, Taiwan

[17]State Key Laboratory of Bioorganic and Natural Products Chemistry, Center for Excellence in Molecular Synthesis, Shanghai Institute of Organic Chemistry, University of Chinese Academy of Sciences, Chinese Academy of Sciences, 200032 Shanghai, China

Abstract

Adenosine monophosphate–activated protein kinase (AMPK) activity is stimulated to promote metabolic adaptation upon energy stress. However, sustained metabolic stress may cause cell death. The mechanisms by which AMPK dictates cell death are not fully understood. We report that metabolic stress promoted receptor-interacting protein kinase 1 (RIPK1) activation mediated by TRAIL receptors, whereas AMPK inhibited RIPK1 by phosphorylation at Ser^{415} to suppress energy stress–induced cell death. Inhibiting pS415-RIPK1 by *Ampk* deficiency or RIPK1 S415A mutation promoted RIPK1 activation. Furthermore, genetic inactivation of RIPK1 protected against ischemic injury in myeloid *Ampkα1*-deficient mice. Our studies reveal that AMPK phosphorylation of RIPK1 represents a crucial metabolic checkpoint, which dictates cell fate response to metabolic stress, and highlight a previously unappreciated role for the AMPK-RIPK1 axis in integrating metabolism, cell death, and inflammation.

Editor's summary

A critical phosphorylation event links the metabolic state of a cell with control of cell death and inflammation. Adenosine monophosphate–dependent protein kinase (AMPK) is a sensor of the nutrient status and energy state of the cell. Zhang *et al.* found that activated AMPK phosphorylates and inhibits receptor-interacting protein kinase 1 (RIPK1) in nutrient-deprived cells, thus inhibiting cell death and inflammation (see the Perspective by Hardie). Under more prolonged nutrient stress, such inhibition was lost, allowing cell death to ensue. These results also confirm RIPK1's role in cell death caused by ischemia, thus implicating the AMPK-RIPK1 interaction as a potential therapeutic target. —L. Bryan Ray

---

Adenosine monophosphate (AMP)–activated protein kinase (AMPK) is an evolutionary conserved sensor of cellular nutrient status and regulator of energy homeostasis in

eukaryotes (1). In response to increases in intracellular AMP that always accompany decreases in adenosine triphosphate (ATP), AMPK is activated and serves as a metabolic checkpoint (1–4). However, when extensive metabolic stress overrides AMPK-mediated adaptation, it activates cell death (5, 6). The mechanisms by which AMPK modulates cell survival under metabolic stress are not fully understood. Receptor-interacting protein kinase 1 (RIPK1) is a key mediator of cell death and inflammation (7, 8). Activated RIPK1 may mediate receptor-interacting protein kinase 3 (RIPK3) and mixed lineage kinase domain-like (MLKL)–dependent necroptosis or caspase-8–dependent apoptosis upon stimulation of tumor necrosis factor receptor 1 (TNFR1) by tumor necrosis factor–α (TNFα) (9–12). RIPK1 is also activated downstream of the death receptors of Fas (also called CD95), as well as TRAIL receptor 1 (TRAIL-R1, also called DR4) and TRAIL-R2 (also called DR5) in addition to TNFR (13–18). Notably, inhibition of RIPK1 activation is highly effective in protecting against ischemic damage (19, 20). However, it remains unknown whether and how RIPK1 may be activated under ischemic conditions.

Metabolic stress promotes the activation of RIPK1

To this end, we incubated cells with glucose-free medium for various lengths of time. Wild-type (WT) mouse embryonic fibroblasts (MEFs) died after 48 hours of glucose deprivation, whereas most MEFs expressing catalytically inactive RIPK1 (*Ripk1*$^{D138N/D138N}$) survived (Fig. 1A and fig. S1A). Moreover, glucose deprivation increased phosphorylation of RIPK1 (S166), a biomarker of RIPK1 activation (21,22), as well as that of RIPK3 (T231/S232) and MLKL (S345), hallmarks of necroptosis (11), which were all blocked in *Ripk1*$^{D138N/D138N}$ MEFs (Fig. 1, B and C, and fig. S1, B and C). Glucose deprivation activates RIPK1 in multiple cell lines, including colon cancer HT-29 cells, more microglia BV2 cells, human T lymphoyam Jurkat cells, and human U2OS osteosarcoma cells (fig. S1, D to I). Increased insolubility is another hallmark of activated RIPK1, RIPK3, and MLKL (22). In glucose-starved MEFs, the amounts of RIPK1, RIPK3, and MLKL were decreased in a mild-detergent (NP-40)–soluble fraction but increased in an NP-40–insoluble and 6M urea–soluble fraction, which was largely blocked by the *Ripk1*$^{D138N/D138N}$ mutation (Fig. 1C and fig. S1, C, F, and G). We also observed interaction of RIPK1 and RIPK3 in MEFs after glucose starvation (fig. S1J). Glucose deprivation induced apoptosis, as marked by the cleavage of RIPK1 and caspase-3 (CC3) (Fig. 1B and fig. S1K). We exposed cells to various concentrations of glucose and found that only severe energy stress induced necroptosis and apoptosis (Fig. 1D). Prolonged treatment of cells with the glucose analog 2-deoxyglucose (2DG), which blocks cellular glucose utilization by indirectly inhibiting hexokinase, also activated RIPK1 to promote necroptosis (fig. S1L).

RIPK1 promotes cell death through its kinase activity, whereas it inhibits cell death through its scaffold functions (21, 23–25). Unlike *Ripk1*$^{D138N/D138N}$ MEFs, which showed resistance to glucose deprivation–induced cell death, *Ripk1* knockout (KO) MEFs were more sensitive to cell death induced by glucose starvation than were WT MEFs (fig. S2A). However, in Jurkat cells, *RIPK1* deficiency decreased cell death and the activation of RIPK3 and MLKL induced by glucose starvation (fig. S2, B and C), indicating that the effects of *RIPK1* deficiency on cell death in response to glucose starvation depend on the cellular context. To investigate the role of necroptosis in glucose deprivation–induced cell death, we

deprived WT, *Ripk3*, and *Mlkl* KO cells of glucose for various lengths of time. Deletion of either *Ripk3* or *Mlkl* partially prevented cell death induced by glucose deprivation (fig. S2, D to F). Notably, the loss in viability and the degree of RIPK1 activation were comparable between WT and *Tnfr1/2* double knockout (DKO) cells (fig. S2, G and H), which indicates that glucose deprivation–induced activation of RIPK1 and cell death is independent of the TNFα signaling pathway.

Next we subjected WT mice, $Ripk1^{D138N/D138N}$ mice, and *Tnfr1/2* DKO mice to hepatic ischemia, a condition that causes mouse livers to become pale, enlarged, and damaged (fig. S3, A and B). Histological analysis showed severe inflammatory infiltration and cell death in ischemic WT and *Tnfr1/2* DKO mice but not in $Ripk1^{D138N/D138N}$ mice (Fig. 1E). We detected activation of RIPK1 as determined by p-RIPK1 (S166) immunostaining and cell death as determined by terminal deoxynucleotidyl transferase–mediated deoxyuridine triphosphate nick end labeling (TUNEL) assay in the livers of WT and *Tnfr1/2* DKO mice but not in those of $Ripk1^{D138N/D138N}$ mice (Fig. 1E and fig. S3C). We analyzed the gene expression profiles of whole livers by RNA sequencing (RNA-seq). Compared to WT sham control mice, WT and *Tnfr1/2* DKO mice showed increased expression of genes associated with an inflammatory response, including interferon alpha (*Ifn*-α), transforming growth factor beta (*TGF*-β), C-X-C motif chemokine ligand 10 (*Cxcl10*), C-X-C motif chemokine ligand 2 (*Cxcl2*), and C-C motif chemokine ligand 2 (*Ccl2*) (Fig. 1, F and G, and fig. S3, D and E); and down-regulation of genes involved in oxidation-reduction processes and the transport signaling pathway (fig. S3, F and G). These gene expression abnormalities were largely rescued by genetic inhibition of RIPK1 in $Ripk1^{D138N/D138N}$ mice (Fig. 1, F and G, and fig. S3, F and G). We confirmed the increased production of *Ccl2*, *Cxcl2*, interleukin 1 alpha (*Il1a*), interleukin 1 beta (*Il1b*), and interleukin 6 (*Il6*) by enzyme-linked immunosorbent assay (ELISA), all of which were reduced in the blood of $Ripk1^{D138N}$ mice but not in that of *Tnfr1/2* DKO mice (Fig. 1H). Thus, these results indicate that ischemia promotes RIPK1-dependent cell death and inflammation in a TNFα-independent manner.

We next explored the possible roles for other death receptors including Fas, DR4, and DR5 in the regulation of RIPK1 activity upon glucose starvation. Deletion of *DR4* or *DR5* but not *FAS* reduced RIPK1 activation and cell death (fig. S4, A to F). Glucose deprivation activates TRAIL receptors through an activating transcription factor 4 (ATF4) and C/EBP homologous protein (CHOP)–dependent mechanism, which promotes cell death in a ligand-independent manner (26). Consistently, we observed increased up-regulation of TRAIL receptors after glucose starvation (fig. S4, D and F). We used the liver ischemia injury mouse model to examine the role of *Dr5*, which is the single TRAIL receptor expressed in mice (27). *Dr5* deficiency suppressed RIPK1 activation, cell death, and inflammation (fig. S4, G and H). Thus, our data demonstrate that TRAIL receptors function as upstream drivers for RIPK1 activation and cell death under glucose deprivation conditions.

AMPK phosphorylates RIPK1 in response to metabolic stress

AMPK is a highly conserved sensor of cellular energy status, which is activated under conditions of low cellular energy such as glucose deprivation (28). RIPK1 derived from cells exposed to glucose deprivation showed a profound RIPK1 mobility shift on standard SDS–

polyacrylamide gel electrophoresis (SDS-PAGE), which was diminished by the treatment of the protein with lambda-phosphatase. Thus, glucose deprivation appears to induce RIPK1 phosphorylation (Fig. 2, A and B, and fig. S5, A and B). Moreover, this glucose deprivation–induced RIPK1 mobility shift was not reversed by RIPK1-specific inhibitor necrostatin-1s (Nec-1s) (19) (fig. S5, C to E). These data indicate that glucose deprivation–induced RIPK1 phosphorylation is not entirely dependent on RIPK1 autophosphorylation. In keeping with this notion, cells expressing RIPK1 catalytically inactive mutant (K45M) (29) showed a strong upshifted band, which was diminished in *AMPK* DKO cells, indicating that AMPK might target RIPK1 for phosphorylation (fig. S5F). We conducted mass spectrometry analysis of RIPK1 phosphorylation under glucose starvation conditions and found that Ser^{416} of RIPK1 is likely a specific phosphorylation site in response to glucose deprivation (fig. S6, A and B). Further sequence analysis showed that the RIPK1 Ser^{416} residue conforms to the AMPK substrate motif validated in some previously identified AMPK substrates (30) (fig. S6C) and represents an evolutionarily conserved residue in human, rat, and mouse (fig. S6C).

To examine endogenous RIPK1 phosphorylation, we developed a phosphospecific antibody against p-S416 of human RIPK1, which corresponds to p-S415 of mouse RIPK1 (fig. S6, D and E). p-S416 of RIPK1 was increased in response to a constitutively active AMPKα1 allele (31) (fig. S7A). We observed increased endogenous p-S415 of murine RIPK1 or p-S416 of human RIPK1 in WT but not in *Ampk* DKO MEFs and HT29 cells, respectively, after glucose starvation (Fig. 2, C and D). We tested whether direct pharmacological activation of AMPK was sufficient to induce phosphorylation of RIPK1. Phosphorylation of RIPK1 at Ser^{415} was induced by the treatment with AMP-mimetic aminoimidazole carboxamide riboside (AICAR) in an AMPK-dependent manner (Fig. 2E and fig. S7B). Similarly, treatment with compound 991, a small molecule that directly binds to and activates AMPK (32), was sufficient to induce RIPK1 phosphorylation at Ser^{415} (Fig. 2F). Consistently, phosphorylation of RIPK1 was also increased in response to treatment with metformin, a widely prescribed drug for type 2 diabetes that is known to activate AMPK both in vitro and in vivo (33) (Fig. 2G and fig. S7, C and D).

Liver kinase B1 (LKB1) is the major kinase that activates AMPK under conditions of energy stress (34). Treatment with metformin or glucose starvation resulted in the phosphorylation of RIPK1 at Ser^{415}, which was abolished in *Lkb1* KO MEFs (fig. S7, E and F). The phosphorylation of $RIPK1^{S415}$ in these cells paralleled the phosphorylation of a well-established AMPK substrate, acetyl–coenzyme A carboxylase (ACC) (Fig. 2, C to G, and fig. S7, C and D) (35). Phosphorylation quickly returned to basal levels when cells were re-stimualted with 25 mM glucose after glucose deprivation for 4 hours (Fig. 2H and fig. S7G). We therefore tested whether AMPK might directly phosphorylate RIPK1. We detected a physical interaction between overexpressed Flag-tagged RIPK1 and hemagglutinin (HA)–tagged AMPK (fig. S7H). Recombinant AMPK induced phosphorylation of Flag-tagged RIPK1 at Ser^{416} or a myelin basic protein fusion with a RIPK1 fragment (390–436) in an in vitro kinase assay (Fig. 2I and fig. S7I). Furthermore, we used ^{32}P-labeled ATP in an in vitro kinase assay (36). The inactive Flag-tagged RIPK1 K45M mutant or glutathione *S*-transferase (GST) fusion of RIPK1 fragment (390–436) was phosphorylated by AMPK (fig. S7, J and K). The stoichiometry of the phosphorylation of RIPK1 at Ser^{416}

by AMPK was estimated to be 0.51 mol phosphate per mol of RIPK1 fragment (390–436). AMPK-mediated incorporation of ^{32}P into RIPK1 was not observed for the RIPK1 fragment containing the S416A mutation (fig. S7K), indicating that AMPK predominantly phosphorylates RIPK1 at Ser^{416}. Furthermore, we detected RIPK1 p-S415 in mouse tissues including lung and brain (fig. S7L). Moreover, in mice subjected to fasting, which causes low glucose in vivo (fig. S7M) (37), RIPK1 p-S415 was increased in liver and pancreas, two organs that are sensitive to fasting, a condition in which AMPK is activated (Fig. 2J and fig. S7N).

Ampk deficiency promotes RIPK1-driven cell death and inflammation

We tested whether phosphorylation of RIPK1 by AMPK represents a survival mechanism in response to glucose deprivation. *Ampk* deficiency sensitized cells to glucose deprivation–induced cell death (Fig. 3A and fig. S8A). Moreover, genetic deletion of *Ampk* in MEFs promoted activation of RIPK1 (Fig. 3B). Accordingly, glucose deprivation induced greater association of RIPK3 with immunoprecipitated RIPK1 in *Ampk* DKO MEFs than in WT MEFs, indicating that *Ampk* deficiency promotes RIPK1-driven necroptosis (Fig. 3C). Similar results were obtained in *AMPK* DKO HT-29 cells (fig. S8, B to E). Because the activation of RIPK1 by glucose deprivation induces both necroptosis and apoptosis, and RIPK1-induced apoptosis is caspase-8 dependent (38), we explored the contribution of necroptosis and apoptosis to the glucose deprivation-induced cell death in *Ampk* DKO MEFs. Cell death induced by glucose deprivation in *Ampk* DKO MEFs was reduced by 10 μM pan-caspase inhibitor quinoline-Val-Asp-difluorophenoxymethylketone (QVD-oph) or 3 μM RIPK3 inhibitor GSK'872 (fig. S8, F and G).

To determine the role of AMPK in the regulation of RIPK1 activity in vivo, we measured RIPK1 activation by p-S166 RIPK1 immunostaining in a diverse set of tissues from $Ampka1a2^{f/f};Ubc\text{-}Cre^{ERT2}$ mice that were treated with tamoxifen to induce the deletion of both *Ampka1* and *Ampka2*. Loss of *Ampka1* and *Ampka2* induced RIPK1 activation and increased cell death in multiple tissues, including spleen, kidney, and intestine (Fig. 3D and fig. S9, A to G). We did not observe increased RIPK1 activity in the livers of *Ampka1* and *Ampka2*–deficient mice (fig. S9, H and I). Thus, there may be tissue-specific activation of RIPK1 in mice lacking *Ampka1* and *Ampka2*. Notably, prolonged glucose deprivation or AICAR activation of AMPK overcame the adaptive response and triggered RIPK1 activation and cell death (Fig. 3E and fig. S10A). We also treated MEFs with 2-DG for various lengths of time. Short-term treatment of cells with 2-DG activated AMPK (39) and increased phosphorylation of RIPK1 at Ser^{415} (fig. S10B). However, phosphorylation of RIPK1 at Ser^{415} decreased after prolonged treatment of cells with 2-DG, which caused RIPK1 activation, as determined by p-RIPK1 (S166) (fig. S10B). Thus, modified AMPK-mediated phosphorylation of RIPK1 may contribute to the switch from adaptive homeostasis to cellular demise in cells exposed to prolonged metabolic stress.

Consistent with the notion that AMPK-mediated phosphorylation of RIPK1 directly inhibits its activity, overexpression of RIPK1 S416A mutant led to higher amounts of p-S166 RIPK1 (fig. S11A). We reintroduced WT and S415A mutant of RIPK1 into *Ripk1* KO MEFs. *Ripk1* KO MEFs reconstituted with the RIPK1 S415A mutant were more sensitive to cell

death induced by glucose deprivation than were the cells reconstituted with WT RIPK1 (Fig. 3F and fig. S11B). Treatment of cells with either caspase inhibitor QVD-oph or RIPK3 inhibitor GSK'872 reduced cell death (fig. S11, C and D). To further investigate the physiological importance of AMPK-mediated phosphorylation of RIPK1 in vivo, we generated *Ripk1*$^{S415A/S415A}$ knock-in mice by the CRISPR-Cas9 technology (fig. S11, E and F). *Ripk1*$^{S415A/S415A}$ mutant mice were born in normal Mendelian ratios, and their growth appeared normal (fig. S11, G and H). However, the RIPK1 S415A mutation increased cell death and inflammation (Fig. 3, G to J, and fig. S11I). These results indicate that RIPK1 S415 phosphorylation inhibits RIPK1 activity and blocks cell death in response to energy stress.

We also investigated whether AMPK has a role in restraining RIPK1 activity in the context of TNFα-induced cell death. *Ampk* deficiency had no effect on RIPK1 activation and inflammation induced by TNFα alone or TNFα-SM-164 (TS) or TNFα-SM-164-zVAD.fmk (TSZ) (fig. S12). Moreover, the RIPK1 S415A mutation had no effect on RIPK1 activation, cell death, or inflammation induced by TNFα in combination with SM-164 or zVAD.fmk (fig. S13). Thus AMPK-mediated RIPK1 phosphorylation appears not to affect TNFα-induced cell death and inflammation.

Inhibition of RIPK1 protects against liver ischemia-reperfusion injury in myeloid *Ampk* KO mice

AMPK exerts anti-inflammatory effects, especially in macrophages, as metabolic activity and inflammatory status are directly linked in these cells (40). We conditionally deleted *Ampkα1*, which is the only catalytic subunit isoform expressed in macrophages (41), in myeloid cells using *Ampkα1*$^{fl/fl}$ mice expressing *LysM-Cre* and then crossed these mice with *Ripk1*$^{D138N/D138N}$ mice to generate *Ampkα1*$^{f/f}$;*LysM-Cre*;*Ripk1*$^{D138N/D138N}$ mice. *Ampkα1* expression was blocked in bone marrow–derived macrophages (BMDMs) isolated from *Ampkα1*$^{fl/fl}$;*LysM-Cre* and *Ampkα1*$^{f/f}$;*LysM-Cre*;*Ripk1*$^{D138N/D138N}$ mice (fig. S14A). *Ampkα1*$^{fl/fl}$;*LysM-Cre* mice showed normal liver and body weight, normal amounts of serum alanine aminotransferase (ALT) and aspartate aminotransferase (AST), and normal liver morphology (fig. S14, B to E). Similar to MEFs, *Ampk*-deficient BMDMs showed increased RIPK1 activation when deprived of glucose (fig. S14, F to H).

Next we subjected these mice to liver ischemia-reperfusion (IR) injury (Fig. 4A). *Ampkα1*$^{fl/fl}$;*LysM-Cre* mice showed increased abnormal ALT and AST in serum compared with WT mice (Fig. 4B). Moreover, *Ampkα1*$^{fl/fl}$;*LysM-Cre* mice showed increased infiltration of inflammatory cells, which was reduced in *Ampkα1*$^{fl/fl}$;*LysM-Cre*;*Ripk1*$^{D138N/D138N}$ mice (Fig. 4C and fig. S15, A and B). We also detected increased numbers of p-S166 RIPK1^{+} and TUNEL^{+} cells as well as increased expression of proinflammatory cytokines in the livers of *Ampkα1*$^{fl/fl}$;*LysM-Cre* mice compared with those of WT mice (Fig. 4, D to H). We immunostained liver tissues after IR injury with a phosphospecific RIPK3 antibody validated in previous studies (42). Although we detected a substantial amount of TUNEL^{+} cells in livers of *Ampkα1*$^{fl/fl}$;*LysM-Cre* mice after hepatic IR injury, none of them showed phosphorylation of T231/S232 of RIPK3, indicating the

absence of necroptosis in IR-injured livers (fig. S15C). These data indicate that RIPK1-dependent apoptosis, more so than necroptosis, mediated cell death and inflammation in response to ischemic stress (fig. S15).

Next we transplanted bone marrow from mice in which *Ampk* was deleted in myeloid cells with or without $Ripk1^{D138N/D138N}$ into WT, $Ripk1^{D138N/D138N}$, and $Ripk1^{S415A/S415A}$ mice (fig. S16A) (43). Lethally irradiated WT recipient mice reconstituted with $Ampka1^{f/f}$;*LysM-Cre* bone marrow cells showed increased concentrations of ALT and AST in serum compared with WT recipient mice reconstituted with $Ampka1^{f/f}$ bone marrow cells in response to liver IR injury (fig. S16B). Thus, *Ampka1* deficiency in myeloid cells appears to promote liver damage after hepatic IR injury in a non–cell-autonomous manner. Consistently, $Ripk1^{D138N/D138N}$ recipient mice reconstituted with $Ampka1^{fl/fl}$;*LysM-Cre* bone marrow cells showed decreased concentrations of ALT and AST in serum compared with WT recipient mice reconstituted with $Ampka1^{fl/fl}$;*LysM-Cre* bone marrow cells (fig. S16B). Thus, *Ampka1* deficiency in myeloid cells facilitates RIPK1 activation by IR injury, which promotes liver proinflammatory immune activation and contributes to the development of hepatocellular damage.

To further link the effects of AMPK on cell death and inflammation to RIPK1 phosphorylation at Ser^{415}, we crossed the $Ampka1^{fl/fl}$;*LysM-Cre* mice into the $Ripk1^{S415A/S415A}$ background. $Ampka1^{fl/fl}$;*LysM-Cre;*$Ripk1^{S415A/S415A}$ mice did not show additional increase in IR injury–induced RIPK1 activation, cell death, or inflammation as compared with that of $Ripk1^{S415A/S415A}$ mice (fig. S16, C to E). Thus, the effects of AMPK on cell death and inflammation appear to be predominantly through AMPK-mediated RIPK1 Ser^{415} phosphorylation in the liver IR injury model we used.

Discussion

Our results indicate that phosphorylation-regulated control of RIPK1 activity enables cellular metabolic control of cell death and inflammation in response to metabolic stress (Fig. 4I). In parallel with other substrates of AMPK, AMPK directly inhibits RIPK1 by phosphorylation, which in turn suppresses energy stress–induced cell death and inflammation (fig. S16F). We revealed a delicate and temporal cellular response of RIPK1 to metabolic stress: Cells activate AMPK to suppress RIPK1 activation, allowing survival in the short term under energy stress, whereas over the longer term, as AMPK phosphorylation of RIPK1 is lost, the inhibition is relieved, promoting a switch to activated RIPK1–mediated cell death and inflammation. The work presented here expands our understanding of the interplay between metabolism and cell death regulation, which may help inform the development of therapeutic drugs aimed at preventing ischemia-induced cell death and tissue damage.

Supplementary Material

Refer to Web version on PubMed Central for supplementary material.

ACKNOWLEDGMENTS

We thank M. Kelliher (University of Massachusetts) and M. Pasparakis (University of Cologne, Germany) for providing *Ripk1*$^{D138N/D138N}$ mice and V. Dixit (Genentech) for *RIPK3* KO mice and the antibodies recognizing phosphorylated RIPK3 Thr231/Ser232 (GEN135-35-9).

Funding:

This work was supported in part by NIH grants [CA177910 and R35CA253027 (W.W.); R00 CA194314 (C.C.D.); RO1 AA017729m and R01 AA011576 (G.Sz.); CA236226, CA239660, CA202634, P01 CA250959, and P01 CA120964 (P.S.); and RO1DK124328 and RO1DK133331 (J.M.)], the National Key R&D Program of China (2022YFC2303102 to L.P.; 2022ZD0213200 to D.X.), and the National Natural Science Foundation of China (92253301 to L.P.; 32070737 to D.X.). J.Y. was supported in part by the China National Natural Science Foundation (82188101, 21837004, 91849204, and 92049303). D.X. and J.Y. were supported in part by the Shanghai Municipal Science and Technology Major Project (grant no. 2019SHZDZX02), the Strategic Priority Research Program of the Chinese Academy of Sciences (XDB39030200 to J.Y.; XDB39030600 to D.X.). Y.-R.L. was supported in part by a Career Development Award, Academia Sinica Taiwan (AS-CDA-110-L07), and the Ministry of Science and Technology Taiwan (110-2320-B-001-029-MY2).

Data and materials availability:

RNA-seq data used to support the present study have been deposited in the Gene Expression Omnibus with an access number of GSE173938. The biological material is available upon request to W.W. All data are available in the main text or the supplementary materials.

REFERENCES AND NOTES

1. Hardie DG, Nat. Rev. Mol. Cell Biol 8, 774–785 (2007). [PubMed: 17712357]
2. Hardie DG, Ross FA, Hawley SA, Nat. Rev. Mol. Cell Biol 13, 251–262 (2012). [PubMed: 22436748]
3. González A, Hall MN, Lin SC, Hardie DG, Cell Metab. 31, 472–492 (2020). [PubMed: 32130880]
4. Lin SC, Hardie DG, Cell Metab. 27, 299–313 (2018). [PubMed: 29153408]
5. Green DR, Galluzzi L, Kroemer G, Science 345, 1250256 (2014). [PubMed: 25237106]
6. Shaw RJ et al. Cancer Cell 6, 91–99 (2004). [PubMed: 15261145]
7. Tummers B. et al. Immunity 52, 994–1006.e8 (2020). [PubMed: 32428502]
8. Yuan J, Amin P, Ofengeim D, Nat. Rev. Neurosci 20, 19–33 (2019). [PubMed: 30467385]
9. Xu D. et al. Cell 174, 1477–1491.e19 (2018). [PubMed: 30146158]
10. Sun L. et al. Cell 148, 213–227 (2012). [PubMed: 22265413]
11. Wang H. et al. Mol. Cell 54, 133–146 (2014). [PubMed: 24703947]
12. Green DR, Cell 177, 1094–1107 (2019). [PubMed: 31100266]
13. Pan G. et al. Science 276, 111–113 (1997). [PubMed: 9082980]
14. Pan G. et al. Science 277, 815–818 (1997). [PubMed: 9242610]
15. Kavuri SM et al. J. Biol. Chem 286, 16631–16646 (2011). [PubMed: 21454681]
16. Cullen SP et al. Mol. Cell 49, 1034–1048 (2013). [PubMed: 23434371]
17. Hartwig T. et al. Mol. Cell 65, 730–742.e5 (2017). [PubMed: 28212753]
18. Henry CM, Martin SJ, Mol. Cell 65, 715–729.e5 (2017). [PubMed: 28212752]
19. Degterev A. et al. Nat. Chem. Biol 1, 112–119 (2005). [PubMed: 16408008]
20. Linkermann A. et al. Proc. Natl. Acad. Sci. U.S.A 110, 12024–12029 (2013). [PubMed: 23818611]
21. Degterev A. et al. Nat. Chem. Biol 4, 313–321 (2008). [PubMed: 18408713]
22. Ofengeim D. et al. Cell Rep. 10, 1836–1849 (2015). [PubMed: 25801023]
23. Dillon CP et al. Cell 157, 1189–1202 (2014). [PubMed: 24813850]
24. Green DR, Oberst A, Dillon CP, Weinlich R, Salvesen GS, Mol. Cell 44, 9–16 (2011). [PubMed: 21981915]

25. Weinlich R, Green DR, Mol. Cell 56, 469–480 (2014). [PubMed: 25459879]
26. Iurlaro R. et al. Mol. Cell. Biol 37, e00479–16 (2017). [PubMed: 28242652]
27. Chaudhary PM et al. Immunity 7, 821–830 (1997). [PubMed: 9430227]
28. Kim J, Kundu M, Viollet B, Guan K-L, Nat. Cell Biol 13, 132–141 (2011). [PubMed: 21258367]
29. Meng H. et al. Proc. Natl. Acad. Sci. U.S.A 115, E2001–E2009 (2018). [PubMed: 29440439]
30. Hardie DG, Schaffer BE, Brunet A, Trends Cell Biol. 26, 190–201 (2016). [PubMed: 26616193]
31. Crute BE, Seefeld K, Gamble J, Kemp BE, Witters LA, J. Biol. Chem 273, 35347–35354 (1998). [PubMed: 9857077]
32. Stein BD et al. Cell Rep. 29, 3331–3348.e7 (2019). [PubMed: 31801093]
33. Howell JJ et al. Cell Metab. 25, 463–471 (2017). [PubMed: 28089566]
34. Shaw RJ et al. Proc. Natl. Acad. Sci. U.S.A 101, 3329–3335 (2004). [PubMed: 14985505]
35. Gowans GJ, Hawley SA, Ross FA, Hardie DG, Cell Metab. 18, 556–566 (2013). [PubMed: 24093679]
36. Hawley SA et al. Biochem. J 459, 275–287 (2014). [PubMed: 24467442]
37. Zhang CS et al. Nature 548, 112–116 (2017). [PubMed: 28723898]
38. Newton K. et al. Nature 574, 428–431 (2019). [PubMed: 31511692]
39. Hawley SA et al. Cell Metab. 11, 554–565 (2010). [PubMed: 20519126]
40. Kelly B, O'Neill LA, Cell Res. 25, 771–784 (2015). [PubMed: 26045163]
41. Mounier R. et al. Cell Metab. 18, 251–264 (2013). [PubMed: 23931756]
42. Heger K. et al. Nature 559, 120–124 (2018). [PubMed: 29950720]
43. Dey A. et al. Science 337, 1541–1546 (2012). [PubMed: 22878500]

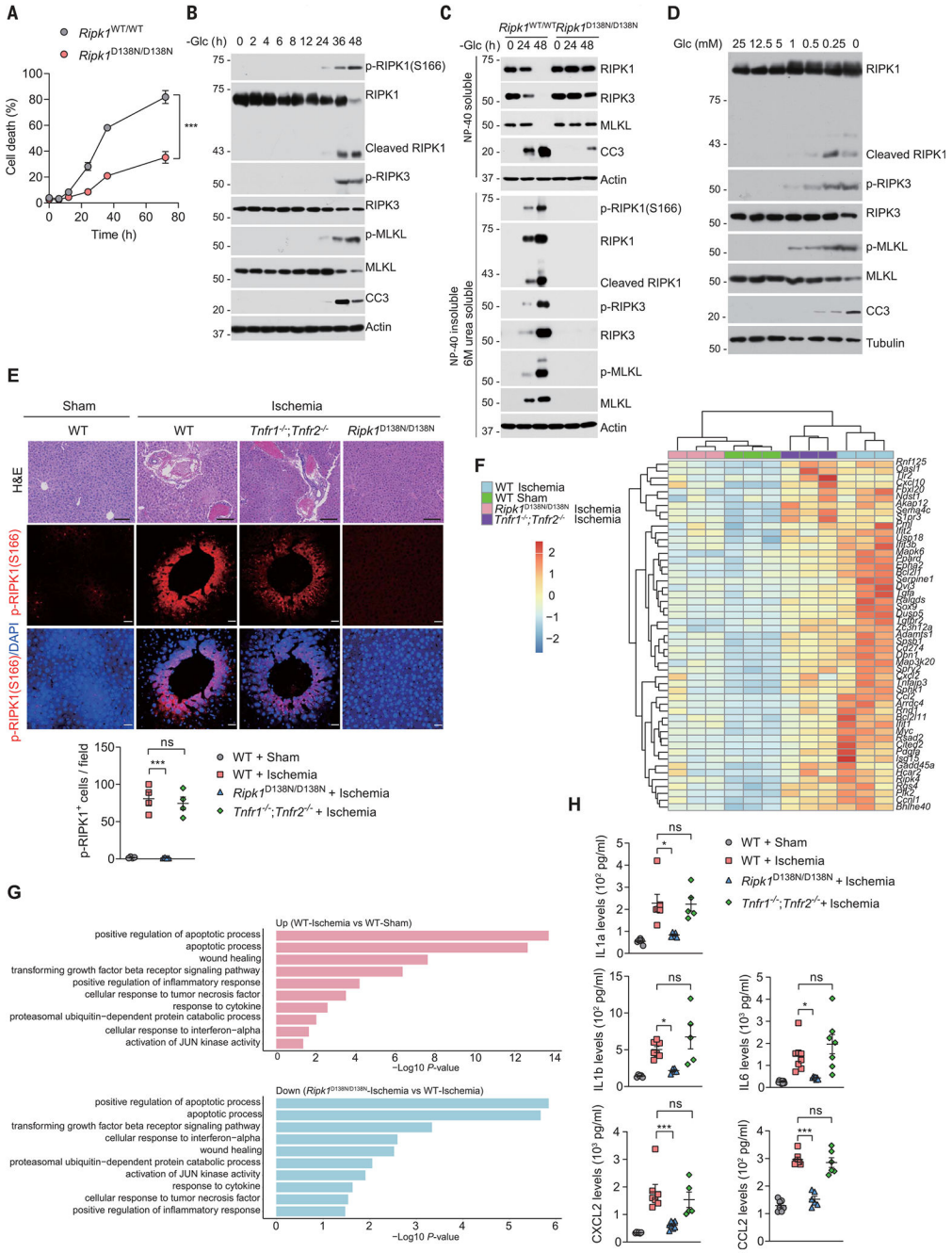

Fig. 1. Metabolic stress promotes cell death and inflammation in a RIPK1-dependent manner.

(**A**) WT or *Ripk1*$^{D138N/D138N}$ MEFs were cultured in glucose-free medium for the indicated times (hours), followed by cell viability analyses using propidium iodide (PI) uptake assay. Data are mean ± SD of $n = 3$ biological independent samples. Two-way analysis of variance (ANOVA); ***$P < 0.001$. (**B**) MEFs were cultured in glucose-free medium for the indicated times. The levels of proteins were determined by immunoblotting. $n = 3$ independent biological repeats. (**C**) WT or *Ripk1*$^{D138N/D138N}$ MEFs were cultured in glucose-free medium for the indicated times. The levels of proteins in

mild-detergent (NP-40)–soluble fraction and 6 M urea–soluble fraction were determined by immunoblotting. $n = 3$ independent biological repeats. (**D**) MEFs were cultured in the medium with different glucose concentrations for 36 hours. The levels of proteins were determined by immunoblotting. $n = 3$ independent biological repeats. (**E**) WT, *Tnfr1/2* DKO, and $Rpik1^{D138N/D138N}$ mice were subjected to a protocol of liver ischemia for 18 hours. Histological analysis and immunostaining for p-RIPK1(S166) were performed on liver sections ($n = 4$ mice in each group). DAPI (4',6-diamidino-2-phenylindole) for nuclei. Representative images are shown. Quantification of p-RIPK1(S166)–positive cells is shown at the bottom. Data are mean ± SEM, one-way ANOVA, post hoc Dunnett's test; $^{***}P < 0.001$; n.s., not significant. Scale bars, 100 μm. (**F**) Heatmap of genes differentially expressed in the whole livers derived of WT, *Tnfr1/2* DKO, and $Rpik1^{D138N/D138N}$ mice subjected to liver ischemia for 18 hours. (**G**) Gene Ontology analysis of genes that are up-regulated in the livers of mice subjected to liver ischemia for 18 hours in a RIPK1-dependent manner. (**H**) ELISA analyses of the levels of indicated cytokines and chemokines in serum from WT, *Tnfr1/2* DKO, and $Rpik1^{D138N/D138N}$ mice subjected to liver ischemia for 18 hours. Data are presented as mean ± SEM, and each dot represents one mouse. One-way ANOVA, post hoc Dunnett's test; $^{*}P < 0.05$, $^{***}P < 0.001$.

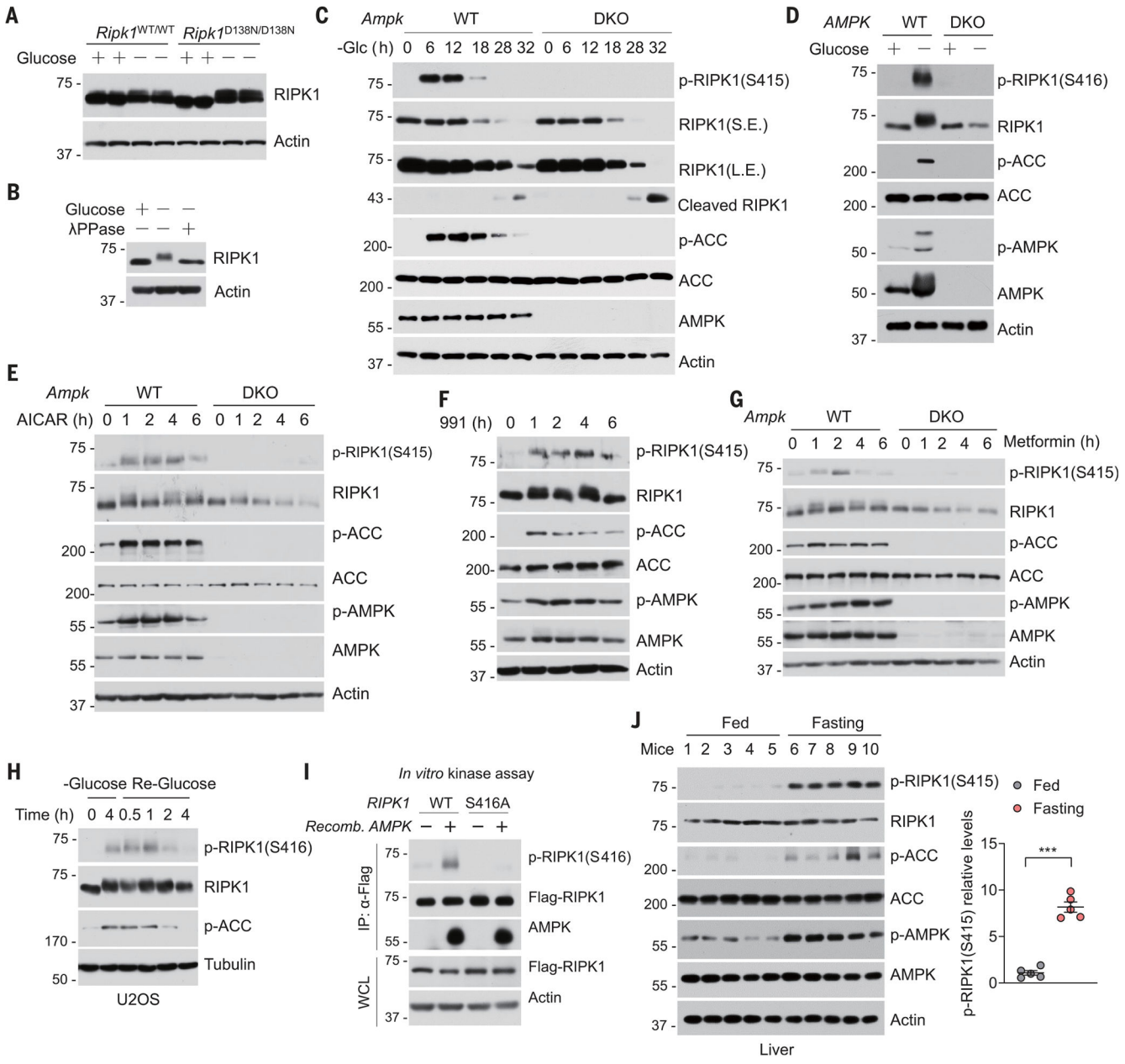

Fig. 2. AMPK phosphorylates RIPK1 at S416 in response to metabolic stress.

(**A**) WT or *Ripk1*$^{D138N/D138N}$ MEFs were cultured in glucose-free medium for 12 hours. Cell lysates were then subjected to immunoblotting using anti-RIPK1 antibody. $n = 3$ independent biological repeats. (**B**) U2OS were cultured in glucose-free medium for 4 hours. Cell lysates were treated with lambda-phosphatase (λPPase), as indicated, for 30 min and then subjected to immunoblotting using anti-RIPK1 antibody. (**C**) WT and *Ampk* DKO MEFs were cultured in glucose-free medium for the indicated times. The levels of proteins were determined by immunoblotting. $n = 3$ independent biological repeats. (**D**) WT and *AMPK* DKO HT-29 cells were cultured in glucose-free medium for 12 hours. The levels of proteins were determined by immunoblotting. $n = 3$ independent biological

repeats. (**E**) WT and *Ampk* DKO MEFs were treated with 2 mM AICAR in the presence of glucose for the indicated times. The levels of proteins were determined by immunoblotting. $n = 3$ independent biological repeats. (**F**) MEFs were treated with 50 μM 991 in the presence of glucose for the indicated times. The levels of proteins were determined by immunoblotting. $n = 3$ independent biological repeats. (**G**) WT and *Ampk* DKO MEFs were treated with 2 mM metformin in the presence of glucose for various times. The levels of proteins were determined by immunoblotting. $n = 3$ independent biological repeats. (**H**) U2OS were starved of glucose (–Glucose) for 4 hours, and then the culture was switched to glucose-containing (25 mM) medium for indicated times (Re-Glucose), and samples were harvested. $n = 3$ independent biological repeats. (**I**) Flag-RIPK1 purified from human embryonic kidney 293T cells expressing Flag-tagged WT or S416A mutant of RIPK1 for 24 hours was combined with recombinant (Recomb.) active AMPK as indicated in an in vitro kinase reaction. The amounts of p-RIPK1 (S416) were determined by immunoblotting. $n = 3$ independent biological repeats. (**J**) Western blot analysis of p-RIPK1 (S415) in livers from fed and fasted (16 hours) animals ($n = 5$). Quantification of p-RIPK1(S415) is shown on the right. Data are presented as mean ± SEM, and each dot represents one mouse. Unpaired two-tailed *t* test; $^{***}P < 0.001$.

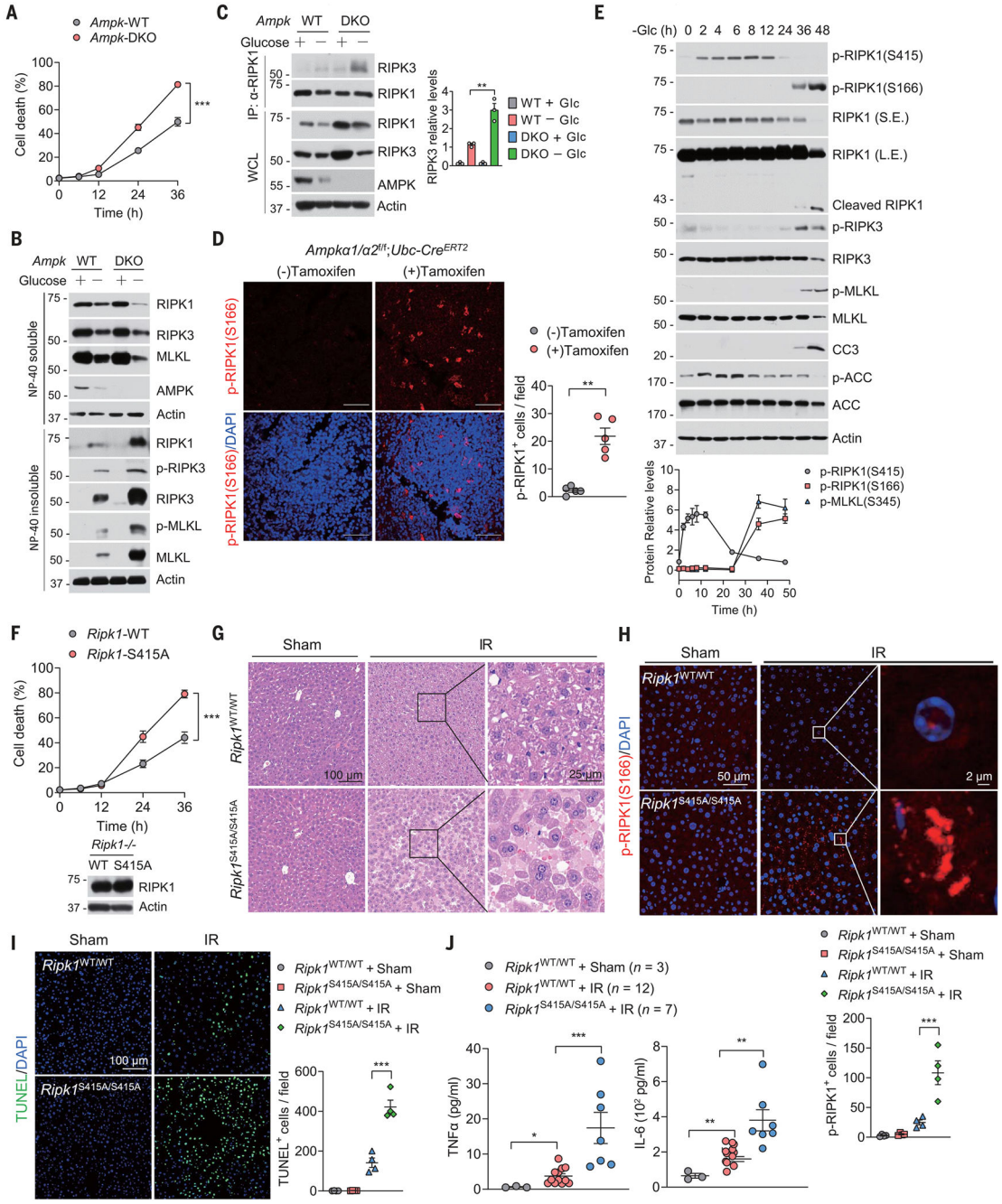

Fig. 3. *AMPK* deficiency promotes RIPK1-driven cell death and inflammation in vitro and in vivo.

(**A**) WT or *Ampk* DKO MEFs were cultured in glucose-free medium for the indicated times followed by cell viability analyses using PI uptake assay. Data are mean ± SD of $n = 3$ biologically independent samples. Two-way ANOVA; ***$P < 0.001$. (**B**) WT or *Ampk* DKO MEFs were cultured in glucose-free medium for 30 hours. The levels of proteins in mild-detergent (NP-40)–soluble fraction and 6 M urea–soluble fraction were determined by immunoblotting. $n = 3$ independent biological repeats. (**C**) WT or

Ampk DKO MEFs were cultured in glucose-free medium for 24 hours. Afterward, cell lysates were immunoprecipitated with anti-RIPK1 antibody, and the immunocomplexes were analyzed by immunoblotting using anti-RIPK3 antibody. $n = 3$ independent biological repeats. Quantified values for Western blot images are shown on the right. $^{**}P < 0.01$. (**D**) *Ampka1/a2*$^{f/f}$*;Ubc-Cre*^{ER} mice were treated with or without tamoxifen (4 mg per day, for 5 days) to induce *Ampk* deletion. Spleens were harvested 8 weeks after tamoxifen treatment, and then immunostaining for p-RIPK1(S166) was performed on spleen sections ($n = 5$ mice in each group). DAPI for nuclei. Representative images are shown. Data are presented as mean ± SEM, and each dot represents one mouse. Unpaired two-tailed *t* test; $^{**}P < 0.01$. Scale bars, 100 μm. (**E**) MEFs were cultured in glucose-free medium for the indicated times. The levels of proteins were determined by immunoblotting. $n = 3$ independent biological repeats. Quantified values for Western blot images are shown at the bottom. (**F**) *Ripk1*$^{-/-}$ MEFs reconstituted with WT or S415A mutant of RIPK1 were cultured in glucose-free medium for the indicated times followed by cell viability analyses using PI uptake assay. Data are mean ± SD of $n = 3$ biological independent samples. Two-way ANOVA; $^{***}P < 0.001$. The expression of RIPK1 was determined by immunoblotting and is shown at the bottom. (**G**) *Ripk1*$^{S415A/S415A}$ and control WT littermate mice were subjected to liver IR injury. Histological analysis on liver sections was performed ($n = 4$ mice in each group). (**H**) *Ripk1*$^{S415A/S415A}$ and control WT littermate mice were subjected to liver IR injury. Immunostaining for p-RIPK1(S166) on liver sections was performed ($n = 4$ mice in each group). DAPI for nuclei. Representative images are shown. Microscopic quantification of p-RIPK1(S166)–positive cells is shown at the bottom. Data are presented as mean ± SEM, and each dot represents one mouse. One-way ANOVA, post hoc Dunnett's test; $^{***}P < 0.001$. (**I**) TUNEL assays were performed on liver sections from *Ripk1*$^{S415A/S415A}$ and control WT littermate mice subjected to liver IR injury ($n = 4$ mice in each group). DAPI for nuclei. Representative images are shown. Microscopic quantification of TUNEL-positive cells was shown on the right. Data are presented as mean ± SEM, and each dot represents one mouse. One-way ANOVA, post hoc Dunnett's test; $^{***}P < 0.001$. (**J**) ELISA analyses of the concentrations of indicated cytokines and chemokines in serum from *Ripk1*$^{S415A/S415A}$ and control WT littermate mice subjected to liver IR injury ($n = 4$ mice each group). Data are presented as mean ± SEM, and each dot represents one mouse. One-way ANOVA, post hoc Dunnett's test; $^{**}P < 0.01$, $^{***}P < 0.001$.

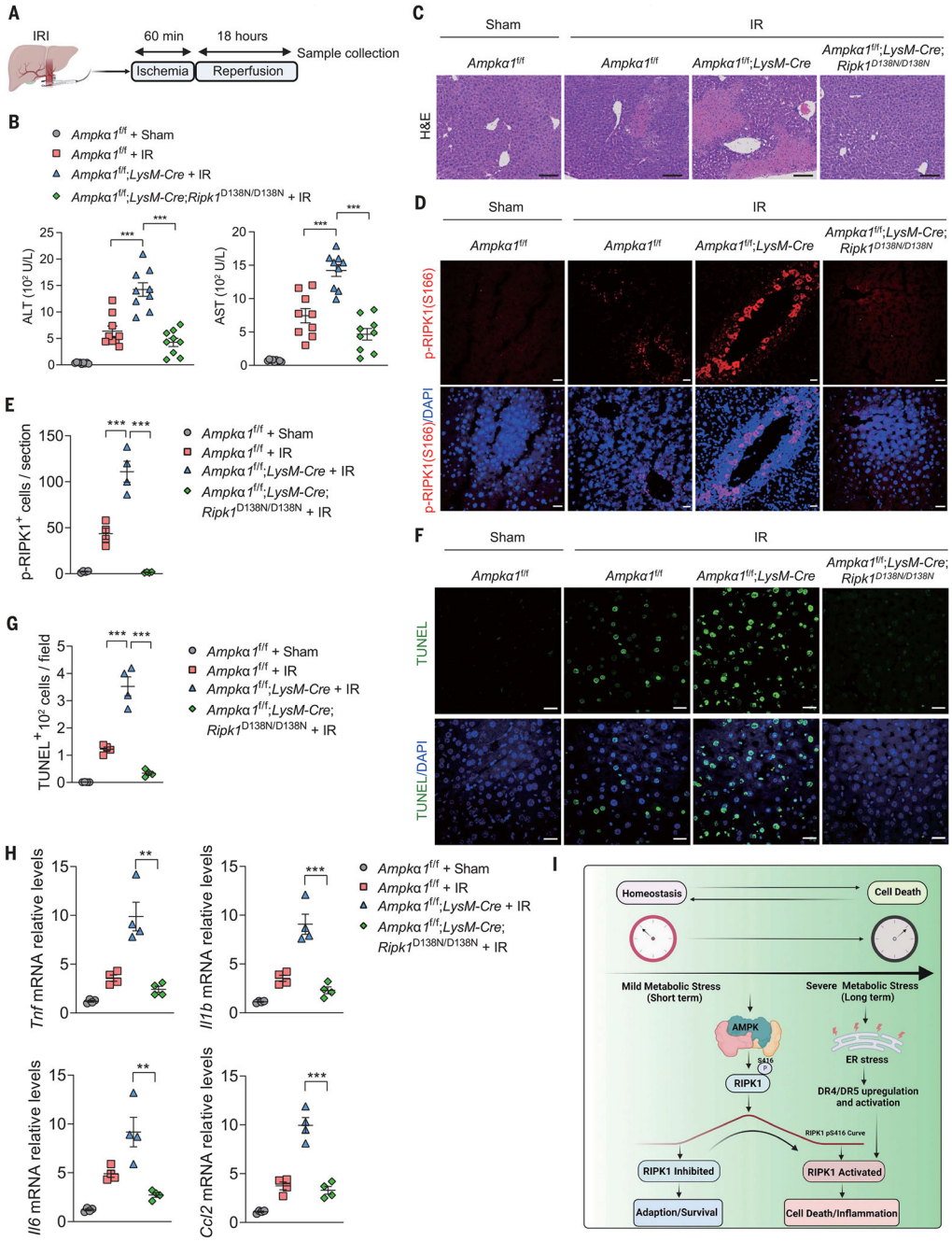

Fig. 4. Inhibition of RIPK1 activity protects against liver IR injury in myeloid *Ampk* KO mice.

(**A**) Schematic of liver IR injury involving 60 min of global ischemia followed by an 18-hour reperfusion period. (**B**) Serum ALT and AST levels were measured from control ($n = 9$), *Ampkα1$^{f/f}$;LysM Cre* ($n = 9$), and *Ampkα1$^{f/f}$;LysMCre;Ripk1$^{D138N/D138N}$* ($n = 9$) mice subjected to liver IR injury. Data are presented as mean ± SEM, and each dot represents one mouse. One-way ANOVA, post hoc Dunnett's test; ***$P < 0.001$. (**C**) Histological analyses were performed on liver sections of *Ampkα1$^{f/f}$;LysM Cre, Ampkα1$^{f/f}$;LysM Cre;Rpk1*$^{D138N/D138N}$, and control littermate mice subjected to liver IR injury ($n =$

4). Representative images are shown. Scale bars, 100 μm. (**D**) Immunostaining for p-RIPK1(S166) was performed on liver sections of *Ampka1*$^{f/f}$*;LysM Cre, Ampka1*$^{f/f}$*;LysM Cre;Ripk1*$^{D138N/D138N}$, and control littermate mice subjected to liver IR injury (n = 4). DAPI for nuclei. Representative images are shown. Scale bars, 100 μm. (**E**) Quantification of p-RIPK1(S166)–positive cells on liver sections from (D). Data are presented as mean ± SEM, and each dot represents one mouse. One-way ANOVA, post hoc Dunnett's test; ***P < 0.001. (**F**) TUNEL assays were performed on liver sections of *Ampka1*$^{f/f}$*;LysM Cre, Ampka1*$^{f/f}$*;LysM Cre;Ripk1*$^{D138N/D138N}$, and control littermate mice subjected to liver IR injury (n = 4). DAPI for nuclei. Representative images were shown. Scale bars, 100 μm. (**G**) Quantification of TUNEL-positive cells on liver sections from (F). Data are presented as mean ± SEM, and each dot represents one mouse. One-way ANOVA, post hoc Dunnett's test; ***P < 0.001. (**H**) Quantitative reverse transcription polymerase chain reaction analysis of the mRNA expression of cytokines and chemokines in livers from control (n = 4), *Ampka1*$^{f/f}$*;LysM Cre* (n = 4), and *Ampka1*$^{f/f}$*;LysM Cre;Ripk1*$^{D138N/D138N}$ (n = 4) mice subjected to liver IR injury. Data are presented as mean ± SEM, and each dot represents one mouse. One-way ANOVA, post hoc Dunnett's test; **P < 0.01, ***P < 0.001. (**I**) A schematic model to illustrate a delicate and temporal cellular response of RIPK1 to metabolic stress: Cells activate AMPK to suppress RIPK1 activation, allowing survival under energy stress in the short term, whereas over longer time periods, as the AMPK phosphorylation of RIPK1 is lost, the inhibition is relieved, promoting a switch to activated RIPK1-mediated cell death and inflammation. Moreover, long-term glucose starvation causes the ATF4/CHOP-dependent up-regulation and activation of TRAIL receptors DR4 and DR5, which promotes RIPK1 activation, cell death, and inflammation.